Transfer path analysis of a railway vehicle based on global transfer direct transfer

Yingli Li, Yong Wang, Juliana Wada

Transfer path analysis of a railway vehicle based on global transfer direct transfer

Yingli Li*

Key Laboratory of Traffic Safety on Track (Central South University),
Ministry of Education,
School of Traffic and Transportation Engineering,
Central South University,
Changsha, 410075, China

and

Joint International Research Laboratory
of Key Technology for Rail Traffic Safety,
Central South University,
Changsha, China
Email: liyingli@csu.edu.cn
*Corresponding author

Yong Wang

Key Laboratory of Traffic Safety on Track (Central South University),
Ministry of Education,
School of Traffic and Transportation Engineering,
Central South University,
Changsha, 410075, China

and

National & Local Joint Engineering Research Center of Safety
Technology for Rail Vehicle,
Central South University,
Changsha, 410075, China
Email: csu_wy@csu.edu.cn

Juliana Wada

Key Laboratory of Traffic Safety on Track (Central South University),
Ministry of Education,
School of Traffic and Transportation Engineering,
Central South University,
Changsha, 410075, China
Email: JulianaWada@csu.edu.cn

Abstract: To overcome the shortcomings of the classical transfer path analysis (TPA) and operation transfer path analysis (OTPA), the global transfer direct transfer (GTDT) method is adopted. This method does not require force determination, and direct transfer functions (DTFs) can be used to identify problematic subsystems, which are calculated and used to determine the cause of the total displacements on the railway vehicle body. When studying the contribution of each component of the bogie to the vehicle body displacements, the effect of different mechanical property parameters is analysed to find the problematic subsystem that causes the highest displacement for improvement. It is creative that mathematical mechanical modelling of a railway vehicle with 6 and 11 degrees of freedom (DOF) is developed for GTDT analysis. Results show that the GTDT method is a promising method for studying the vibration transmission path of complex practical rail vehicle systems. It can diminish the vibration efficiently.

Biographical notes: Yingli Li, Associate Professor, Doctoral Supervisor, Graduated from Hunan University (2003–2013), majoring in Mechanics, joint PhD at the University of Toronto, Canada, and postdoctoral fellowship at Nanyang Technological University, Singapore. Now, she is mainly engaged in the research of vibration and noise reduction of rail transportation equipment. She has published 70 academic papers, including 60 papers in international journals, which have been cited more than 1000 times, with h-Index of 16.

Yong Wang received his Master's degree in 2022, with research interests in noise and vibration control, metamaterial design and optimisation.

Juliana Wada received her Master's degree in 2020 for research on vibration transmission paths.

1   Introduction

The vibration and noise impact in the railway system have been issues of concern for many years (Moghaddam, 2017, Wei et al., 2019, Jin et al., 2020) intending to improve the effect of it on the surrounding environment and humans. Reducing railway vehicles' noise and vibration can lead to an increase in product lifetime, and improvement in ergonomics and human ride comfort. It is necessary to identify the sources and transfer paths of vibration and noise to improve it.

Many studies have identified the interaction between wheel and rail during running as a vital vibration source (Ling et al., 2020). Also, bridge noise (Liu et al., 2020b), aerodynamic noise (Cao et al., 2021), air conditioning fan noise (Lv et al., 2021), and other types of sources (Liu, 2020) have been recognised. Another critical point is to figure out the contribution of every kind of vibration and noise source to the receiver and apply corresponding measures for mitigation (Xia et al., 2021).

The demand for reducing vibration and noise led to the development of different types of transfer path analysis (TPA) methods (Meggitt et al., 2021). TPA can identify the transmission path of noise and vibration from the excitation source to the receiving point and analyse the contribution of each path. It finds out the main path of vibration transmission, and then we can improve the structure to reduce or eliminate the noise or vibration of the mechanical structure.

Several methods for the TPA have been studied from theoretical developments to practical techniques, and they are still under improvement. The traditional TPA method takes up a large proportion in the automotive industry (Zhang et al., 2019). It can establish an exact and complex mathematical physical model, but its implementation is challenging. First, it needs to disassemble the active parts one by one; secondly, it needs to carry out experiments in professional laboratories. Therefore, this method does not apply to the TPA of a railway vehicle.

Several other methods for the TPA have then emerged, among which the operational transfer path analysis (OTPA) (Song et al., 2021) and advanced transfer path analysis (ATPA) (Aragonès et al., 2019) are two applicable ones for railway vehicles. OTPA is a very convenient method because it is an operational method that does not need to disassemble parts. However, it cannot avoid the crosstalk and coupling of adjacent signals.

The ATPA method regards the global transfer direct transfer (GTDT) method. In this method, the global and direct transfer functions (DTFs) among subsystems in a linear network are obtained first under steady operational conditions. Then the analysis is extended to a functional case to study the contribution of each subsystem. In this method, no force determination is necessary, and it is possible to identify the problematic subsystems using DTFs avoiding crosstalk. Therefore, in this paper, the GTDT method is applied to study the contribution of each subsystem of the railway vehicle to the overall vibration of the vehicle body and bogie.

Some significant works have been done focusing on different TPA methods. In 2008, Guasch (2009) proposed the GTDT method in a mechanical system when blocking transmission paths, which was proved to be a non-intrusive alternative with less experimental efforts. de Klerk and Ossipov (2010) studied the OTPA using singular value decomposition (SVD) and analysed vehicle tyre noise. In 2016, a general framework for TPA was suggested (van der Seijs et al., 2016), which can be considered as a very essential fundament for the understanding of many possibilities and combinations of TPA practices. An overview (Oktav et al., 2017) of methods was proposed in 2017, revealing its drawbacks, advantages, and assumptions for an engine-induced structure-borne noise. Concerning the OTPA method, an alternative formulation called operational transfer path analysis-difference (OTPA-D) (Vaitkus et al., 2019) was proposed in 2019. In 2020, an emerging deep neural network model was presented and uses the operational responses to identify the contributions of all paths in the frequency domain (Lee and Lee, 2020). The paper provides a comparison among TPA, OTPA, and OTPA-D methods in the analytical and laboratory model. In the same year, the ATPA method was applied in a box with an air cavity inside as a laboratory prototype and a numerical model was developed to compare with the laboratory measurement response (Aragonès et al., 2019).

Concerning the railway vehicle, the OTPA has been applied and drawbacks to OTPA are the coherence among input signals (Liu et al., 2020a). As for the GTDT method, although its theory had developed since the 1980s (Magrans, 1981, 1984), the application

in the railway vehicle is still limited. This paper will extend the GTDT method to the vibration TPA of a railway vehicle.

The importance of this paper is to investigate the vertical vibration transfer path contribution of a railway vehicle system, modelled as 6 DOF and 11 DOF mass-spring mechanical systems for a half and entire vehicle, respectively. The effect of parameter changes on the global and DTF is discussed. The interaction contact between the rail and the wheel is taken as the excitations of the system to study the contribution of each transfer path to the vibration and noise of the vehicle.

This paper highlights the main advantage of using the GTDT method in a mechanical system, as the displacement contributions can be obtained utilising DTFs. The DTFs are obtained to find the complex subsystems that cause the highest portions of displacements. Therefore, the results can provide suggestions on which component or subsystem has more contribution to the total vibration of the system.

In Section 2, the GTDT method is introduced, focusing on the construction of transfer functions and the factorisation method. In sections 3 and 4, the two steps of the GTDT method are applied to the 6 DOF and 11 DOF models of railway vehicles, respectively. The frequency responses of global and DTFs are obtained, and the effect of system parameters change on the transfer function is discussed among the different cases. Afterwards, the operational displacements of each mass are obtained, and the contribution among directly connected subsystems is discussed. Section 5 is the conclusion of the paper.

2   Advanced transfer path analysis (ATPA) based on global transfer direct transfer (GTDT)

The GTDT method presents two types of transfer functions, DTF and global transfer function (GTF). This method regards the TPA among subsystems in a linear network first under steady operational conditions and then extended to the operational case. The first step of the method is to find the GTFs by simulation or experiments. Then, the DTF obtains from the GTFs according to the network system characteristics. The direct transfer matrix plays the role of the connection matrix.

Another critical point of the method is that it involves two steps. It involves reconstructing signals in any subsystem through DTF and working conditions, and then obtaining the signals in other subsystems. This will allow effortlessly identifying which subsystem is not working properly and guide how to correct the impact of this signal on the overall system. This method also avoids the need to disassemble parts and measure force.

2.1   Definition of direct transfer function (DTF) and global transfer function (GTF)

The definition of DTF and GTF can be found in Magrans (1981, 1984). The GTF T_{ij}^G at frequency ω is the transfer function between signals s_i and s_j in 2 subsystems i and j, when subsystem i is subjected to an external excitation $\hat{f}_i^{ext}$:

$$T_{ij}^G(\omega) = s_j(\omega)/s_i(\omega), \hat{f}_i^{ext}(\omega) \neq 0, \hat{f}_k^{ext}(\omega) = 0, k = 1,2,3,...,i-1,i+1,...,n \qquad (1)$$

According to the equation above, the GTF is the portion of the signal of subsystem i to subsystem j via all possible paths or global paths. For this reason, the GTF consider all set of paths, called Global Transmission Path, in the GTDT. The Global Transfer Matrix $\mathbf{T}^G$ of all the pairs of subsystems in the system network can be built from equation (1).

The significance of this transfer function is that the signal j is not transmitted just between i and j directly, but also through many other paths that link these two subsystems. The DTF is defined as the transfer function between subsystems i and j directly.

After GTF is calculated from the system frequency response signals, the DTF is obtained based on the GTF. The DTF is the quotient between the signal i and signal j when an excitation f_i^{ext} is applied to subsystem i and transmitted via the direct path to subsystem j while all the other signals main 0. For this reason, the change in DTF permits knowing the consequences of property change in one subsystem over another subsystem without considering the rest of the network. The DTF T_{ij}^D is defined as the signal transmitted directly from one subsystem to another:

$$T_{ij}^D(\omega) = s_j(\omega) / s_i(\omega), f_i^{ext}(\omega) \neq 0, \ s_k = 0, k \neq i \tag{2}$$

DTF T_{ii}^D is the quotient between the signal $s_i^{'}$ and signal s_i^{ext}, with an external excitation f_i^{ext} applied in i and all other signals main 0. The signal s_i^{ext} is obtained by the same excitation applied to i and no restrictions on the other subsystem signals. In case the signal is transmitted to i via global path:

$$T_{ii}^D(\omega) = \frac{s_i^{'}(\omega)}{s_i^{ext}(\omega)}, \begin{cases} for \ s_i^{'}(\omega): f_i^{ext}(\omega) \neq 0, s_k = 0 \\ for \ s_i^{ext}(\omega): f_i^{ext}(\omega) \neq 0, f_k^{ext}(\omega) = 0 \end{cases}, k = 1, 2, 3, ..., i-1, i+1, ..., n \tag{3}$$

The signal i is caused by $f_i^{ext}(\omega)$ and other response contributions of all remaining subsystems. Also $s_i^{'}(\omega)$ is the fraction of s_i^{ext} and it is only due to f_i^{ext} at $.i$. The DTF between two subsystems without a direct link will be zero and the transfer function for the two subsystems linked are non-zero. The DTF matrix also can be regarded as a connectivity matrix, as shown in Aragonès et al. (2019).

The direct transfer matrix $\mathbf{T}^D$ can be obtained from equations (2) and (3). Equation (2) gives the off-diagonal elements T_{ij}^D and equation (3) gives the diagonal elements T_{ii}^D of the matrix $\mathbf{T}^D$.

After matrix $\mathbf{T}^D$ is obtained, the first step of the method is finished.

The second step is to reconstruct the operational signal in any subsystem, in terms of external signal s^{ext} and signals in the remaining subsystems. Therefore, the external signal s^{ext} can be got from measurable quantities, as the operational signal vector s and matrix T^G as follows:

$$s^{ext} = \left(\mathbf{T}^{G^T} \right)^{-1} s \tag{4}$$

The signal vector $s(\omega)$ in the remaining subsystems is related to the external signal $s^{ext}(\omega)$ as follows:

$$s = \left(\text{dev}\mathbf{T}^D\right)^T s + \mathbf{\Lambda}_{TD} \, s^{ext} \tag{5}$$

Matrix $\mathbf{\Lambda}_{TD}$ is the relation between the GTFs and DTFs matrices given by:

$$\mathbf{T}^G \mathbf{T}^{DE} = -\mathbf{\Lambda}_{TD} \; . \tag{6}$$

$$\mathbf{T}^{DE} = \text{dev}\mathbf{T}^D - \mathbf{I} \tag{7}$$

where $\mathbf{I}$ is the identity matrix and $\text{dev}\mathbf{T}^D$ the deviatoric part of $\mathbf{T}^D$ as defined in (Guasch, 2009).

The mathematical relationship between $\mathbf{T}^D$ and $\mathbf{T}^G$ are explored in (Magrans, 1981, Magrans, 1984) and defined as

$$\frac{1}{T_{ii}^D} = -\mathbf{T}^{DE} \mathbf{\Lambda}_{TD}^{-1} \big|_{ii} \tag{8}$$

$$-\frac{\mathbf{T}_{ij}^D}{\mathbf{T}_{ii}^D} = -\mathbf{T}^{DE} \mathbf{\Lambda}_{TD}^{-1} \big|_{ij} , i \neq j \tag{9}$$

2.2   Factorisation method

The direct transfer matrix $\mathbf{T}^D$ can be used to factorise the response of each subsystem in terms of responses due to the force acting on it plus the responses due to the other subsystems.

To find out the operational signals of each subsystem, X^{OP}, due to operational forces:

$$X^{op} = \left(\text{dev}T^D\right)^T X^{op} + \mathbf{\Lambda}^D X^{op,ext} \tag{10}$$

where $\text{dev}\mathbf{T}^D$ represents the off-diagonal elements of the direct transfer matrix $\mathbf{T}^D$, $\mathbf{\Lambda}^D$ is the diagonal elements of $\mathbf{T}^D$. $X^{op,ext}$ is the operational external signal vector. It contains the signals of each subsystem exclusively due to the external forces acting on it, written as:

$$X^{op,ext} = \left[\left(\mathbf{T^G}\right)^T\right]^{-1} X^{op} \tag{11}$$

So, to obtain the contribution of each source in the total signal in a chosen subsystem, the DTFs between subsystems directly linked must be obtained. Equation (12) allows locating the most significant vibration source in a mechanical system.

3 ATPA analysis of the railway vehicle with 6 DOF model

This section is dedicated to implementing the ATPA method to analyse the vertical displacements of a mechanical system as a railway vehicle. A mathematical model of half vehicle represented by 6 DOF is proposed and four cases with different structure parameters are compared and discussed. The purpose is to show the effect of stiffness and masses change on the response of the vehicle body. It studies the effects of the decrease of masses due to reprofile and stiffness change due to manufacture's error during production or performance deterioration during the lifetime.

The external force simulating the wheel-rail interaction is applied as excitation on the wheelset, as the rolling contact force is the primary vibration and noise source. The Global and DTFs between subsystems are obtained based on the theory in Section 2. The operational response vertical displacement is found by the factorisation method, and the curves of displacement amplitude among connected subsystems are also displayed.

3.1 Mathematical model of a half railway vehicle with 6 DOF

In this study, half of a railway vehicle is modelled as a 6 DOF mechanical system considering the symmetry of the front and rear parts of the vehicle, as shown in Figure 1. In the model, mass M_1 represents the half vehicle body, mass M_2 means the bogie, and masses M_3, M_4, M_5, and M_6 stand for the wheels. The vehicle body M_1 is sustained by the secondary suspension modelled as two springs in parallel with total stiffness k_{12}. The bogie frame M_2 is supported by the primary suspension modelled as 4 springs with stiffness k_{23}, k_{24}, k_{25} and k_{26}. The contact stiffness between wheels M_3, M_4, M_5, M_6 and rails are considered with stiffness k_g. The 6 Subsystems in the half vehicle model in Figure 1 are listed in Table 1 regarding the vertical displacements denoted as z_i $(i = 1, 2, , 6)$.

Figure 1 Physical model a half vehicle with 6 DOF
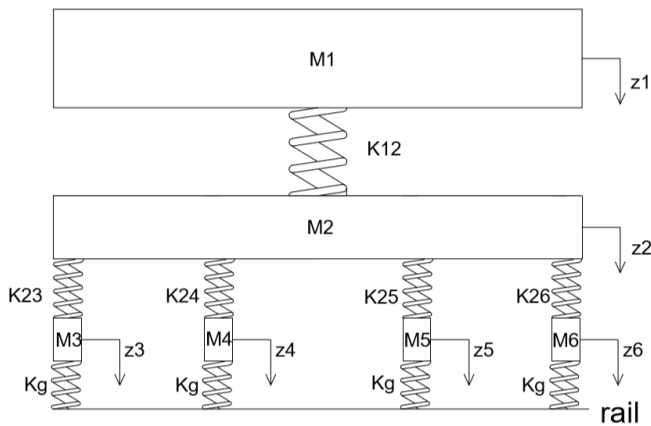
Table 1   Subsystem description

Subsystem number	1	2	3	4	5	6
Subsystems	Half vehicle body	Bogie frame	Wheel 1	Wheel 2	Wheel 3	Wheel 4

The governing equations of motion according to the Newton's second law based on static equilibrium state, are the following:

For the half vehicle body mass M_1:

$$M_1\ddot{z}_1 = F_{12} - f_1$$
$$M_1\ddot{z}_1 = k_{12}(z_1 - z_2) - f_1 \tag{12}$$

In equation (12), F_{12} is the restoring force of secondary suspension between the vehicle body and bogie with stiffness k_{12}. M_1 is the half mass of the vehicle body. f_1 is the external force acting on the vehicle body, which might be an aerodynamic force, wind force or excitation from a device mounted over the vehicle body. Also, z_1 is the vehicle body displacement and z_2 is the bogie displacement.

For the bogie mass:

$$M_2\ddot{z}_2 = F_{23} + F_{24} + F_{25} + F_{26} - F_{12} - f_2$$
$$M_2\ddot{z}_2 = k_{23}(z_2 - z_3) + k_{24}(z_2 - z_4) + k_{25}(z_2 - z_5) + k_{26}(z_2 - z_6) - k_{12}(z_1 - z_2) - f_2 \tag{13}$$

For equation (13), F_{23}, F_{24}, F_{25} and F_{26} are the restoring force of primary suspension with stiffness k_{23}, k_{24}, k_{25} and k_{26}. f_2 is the external force acting on the bogie, generated by the excitation of the motor, gearbox and other devices mounted on the bogie. Also, z_3, z_4, z_5 and z_6 are the displacements of each wheel.

Each wheel is under both the contact force of wheel and rail interaction and the restoring force of primary suspension connected to the bogie frame.

For the wheel masses M_3, M_4, M_5 and M_6, we have

$$M_3\ddot{z}_3 = k_g z_3 - F_{23} - f_3$$
$$M_3\ddot{z}_3 = k_g z_3 + k_{23}(z_3 - z_2) - f_3 \tag{14}$$

$$M_4\ddot{z}_4 = k_g z_4 - F_{24} - f_4$$
$$M_4\ddot{z}_4 = k_g z_4 + k_{24}(z_4 - z_4) - f_4 \tag{15}$$

$$M_5\ddot{z}_5 = k_g z_5 - F_{25} - f_5$$
$$M_5\ddot{z}_5 = k_g z_5 + k_{25}(z_5 - z_5) - f_5 \tag{16}$$

$$M_6\ddot{z}_6 = k_g z_6 - F_{26} - f_6$$
$$M_6\ddot{z}_6 = k_g z_6 + k_{26}(z_6 - z_6) - f_6 \tag{17}$$

In equations (14)–(17), f_3, f_4, f_5, and f_6 are the force excitation between the wheel and rail interaction, which come from the rail roughness or wheel irregularities.

3.2 GTF and DTF of 6 DOF model

For the first part of the method, the GTF and the DTF are represented in Figure 2, considering the external force on the wheelsets. Figure 2(a) represents the GTF connections, which shows the Global Transmission Path, and it considers all connections among the six subsystems. Figure 2(b) shows the direct transfer paths between subsystems. The DTF can be got after the GTF are obtained.

Figure 2 (a) Global transfer functions among all subsystems and (b) direct transfer functions between two direct connected subsystems and T_{ii}^D
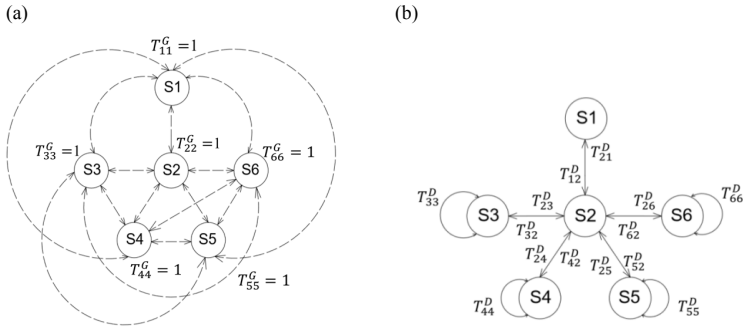
The excitation on the wheel has the form of $f_i = F_i \cos\omega t\,(i = 1,2,\ldots,6)$. The time-harmonic response of the system can be assumed as $z_i = Z_i \cos\omega t$ with frequency ω. Therefore, the equation of motion of the system can be defined as:

$$F = \left(\bar{\mathbf{K}} - \bar{\mathbf{M}}\omega^2\right)Z \tag{18}$$

$Z = \left(Z_1, Z_2, Z_3, Z_4, Z_5, Z_6\right)^T$ is the displacement vector of the six masses, $F = \left(F_1, F_2, F_3, F_4, F_5, F_6\right)^T$ is the force vector. $\bar{\mathbf{M}}$ is the mass matrix of the mass of the four wheels, the bogie frame mass M_2 and the half vehicle body mass M_1 represented by:

$$\bar{\mathbf{M}} = \begin{pmatrix} M_1 & 0 & 0 & 0 & 0 & 0 \\ 0 & M_2 & 0 & 0 & 0 & 0 \\ 0 & 0 & M_3 & 0 & 0 & 0 \\ 0 & 0 & 0 & M_4 & 0 & 0 \\ 0 & 0 & 0 & 0 & M_5 & 0 \\ 0 & 0 & 0 & 0 & 0 & M_6 \end{pmatrix} \tag{19}$$

$\bar{\mathbf{K}}$ is regarded as the complex stiffness matrix, and is defined by:

$$\bar{\mathbf{K}} = \begin{pmatrix} \bar{k}_1 & \bar{k}_{12} & 0 & 0 & 0 & 0 \\ \bar{k}_{12} & \bar{k}_2 & \bar{k}_{23} & \bar{k}_{24} & \bar{k}_{25} & \bar{k}_{26} \\ 0 & \bar{k}_{23} & \bar{k}_3 & 0 & 0 & 0 \\ 0 & \bar{k}_{24} & 0 & \bar{k}_4 & 0 & 0 \\ 0 & \bar{k}_{25} & 0 & 0 & \bar{k}_5 & 0 \\ 0 & \bar{k}_{26} & 0 & 0 & 0 & \bar{k}_6 \end{pmatrix}$$

(20)

For the problem stated:

$$\bar{k}_1 = \bar{k}_{12}; \bar{k}_2 = \bar{k}_{23} + \bar{k}_{24} + \bar{k}_{25} + \bar{k}_{26} + \bar{k}_{12}; \bar{k}_3 = \bar{k}_{23} + \bar{k}_g; \bar{k}_4 = \bar{k}_{24} + \bar{k}_g;$$
$$\bar{k}_5 = \bar{k}_{25} + \bar{k}_g; \bar{k}_6 = \bar{k}_{26} + \bar{k}_g$$

(21)

A dynamic stiffness matrix is defined as:

$$\mathbf{Z}^{SPR} = \bar{\mathbf{K}} - \omega^2 \bar{\mathbf{M}}$$

(22)

For the model in consideration, the matrix $\mathbf{Z}^{SPR}$ will be:

$$\mathbf{Z}^{SPR} = \begin{pmatrix} \bar{k}_1 - M_1\omega^2 & -\bar{k}_{12} & 0 & 0 & 0 & 0 \\ -\bar{k}_{12} & \bar{k}_2 - M_2*\omega^2 & -\bar{k}_{23} & -\bar{k}_{24} & -\bar{k}_{25} & -\bar{k}_{26} \\ 0 & -\bar{k}_{23} & \bar{k}_3 - M_3*\omega^2 & 0 & 0 & 0 \\ 0 & -\bar{k}_{24} & 0 & \bar{k}_4 - M_4*\omega^2 & 0 & 0 \\ 0 & -\bar{k}_{25} & 0 & 0 & \bar{k}_5 - M_5*\omega^2 & 0 \\ 0 & -\bar{k}_{26} & 0 & 0 & 0 & \bar{k}_6 - M_6*\omega^2 \end{pmatrix}$$

(23)

From the matrix (23), denoting the inverse of $\mathbf{Z}^{SPR}$ as $\mathbf{H}^{SPR}$, $\mathbf{H}^{SPR} = \left(\mathbf{Z}^{SPR}\right)^{-1}$, which is called dynamic compliance matrix:

$$X = \mathbf{H}^{SPR} F$$

(24)

The matrix $\mathbf{T}^G$ can be obtained by terms of $\mathbf{H}^{SPR}$, because T_{ij}^G between masses m_i and m_j is given by $F_i H_{ji}^{SPR} = X_j$. T_{ij}^G can be defined as the relation between displacements X_i and X_j. Thus, $T_{ij}^G = X_j / X_i = X_j / F_i / X_i / F_i = H_{ij}^{SPR} / H_{ii}^{SPR}$, the matrix $\mathbf{T}^G$ can be defined as:

$$\mathbf{T}^G = \begin{bmatrix} 1 & \cdots & H_{61}^{SPR} / H_{11}^{SPR} \\ \vdots & \ddots & \vdots \\ H_{16}^{SPR} / H_{66}^{SPR} & \cdots & 1 \end{bmatrix}$$

(25)

In this study, the vehicle is simplified as a mass-spring system with 6 DOF, where the explicit expression for the GTF can be obtained as equation (25). However, the mechanical system of a practical railway vehicle is very complicated, which cannot be simplified as a mechanical system with finite DOF to obtain the GTF explicitly. Thus, actual vehicle tests are carried out to measure the motion of each component, and the

GTF can be obtained according to equation (1). Once the GTF is obtained, the DTF can be obtained based on the relation between the global and direction transfer function in equations (8) and (9).

Equations (2) and (3) are used to obtain the DTF to find the diagonal elements and off-diagonal ones. As the model stated, for the non-diagonal elements of the DTF:

$$T_{13}^D = T_{14}^D = T_{15}^D = T_{16}^D = T_{31}^D = T_{41}^D = T_{51}^D = T_{61}^D = T_{34}^D = T_{43}^D = T_{35}^D = T_{53}^D$$
$$= T_{36}^D = T_{63}^D = T_{45}^D = T_{54}^D = T_{46}^D = T_{64}^D = T_{56}^D = T_{65}^D = 0$$

The matrix T^D, will be the following:

$$T^D = \begin{pmatrix} T_{11}^D & T_{12}^D & 0 & 0 & 0 & 0 \\ T_{21}^D & T_{22}^D & T_{23}^D & T_{24}^D & T_{25}^D & T_{26}^D \\ 0 & T_{32}^D & T_{33}^D & 0 & 0 & 0 \\ 0 & T_{42}^D & 0 & T_{44}^D & 0 & 0 \\ 0 & T_{52}^D & 0 & 0 & T_{55}^D & 0 \\ 0 & T_{62}^D & 0 & 0 & 0 & T_{66}^D \end{pmatrix} \tag{26}$$

For the diagonal elements T_{ii}^D, from equations (8) and (24) as the value of Z^{SPR} known, it can be regarded as:

$$T_{ii}^D = \frac{1}{\left[\left(\bar{k}_i - \omega^2 m_i \right) H_{ii}^{SPR} \right]}, \forall i = 1, 2, 3, 4, 5, 6 \tag{27}$$

For the non-diagonal elements, from equations (9) and (24):

$$T_{ij}^D = \frac{\bar{k}_{ij}}{\left(\bar{k}_j - \omega^2 m_j \right)}, \forall i, j = 1, 2, 3, 4, 5, 6 \ i \neq j \tag{28}$$

The GTF and DTF were analysed and the values of $20 \times \log_{10} \left(T_{ij}^{G,D} \right)$ for pairs of subsystems were discussed.

Four cases with different structure parameters are analysed to investigate the parameter change effect on the system behaviour. Table 2 shows the parameter values of cases (a), (b), (c), and (d). The model with parameters in case (a) is a symmetric one, where all the wheel and corresponding suspension are in an ideal state with the same parameters. In cases (b), (c) and, (d), the stiffness and mass have a little deviation from the ideal state to show the effect of structure parameters change on the transfer function.

In case (a), the value of the secondary suspension k_{12} is ten times bigger than that in case (b). For primary suspension values k_{23}, k_{24}, k_{25} and k_{26} in case (a), are ten times lower than case (b). For case (c), the values of primary and secondary suspension are the same as the case (b), except for the stiffness k_{23}, which is 1.2 times higher than case (b). As for case (d), the values of primary and secondary suspension are the same, but the masses of the wheels M_3 and M_4 are 10% and 15% lower respectively.

Table 2   Variable values

Variables	Case (a)	Case (b)	Case (c)	Case (d)
k_{12}	10^8 N/m	10^7 N/m	10^7 N/m	10^7 N/m
k_{23}	10^7 N/m	10^8 N/m	1.2×10^8 N/m	10^8 N/m
k_{24}, k_{25}, k_{26}	10^7 N/m	10^8 N/m	10^8 N/m	10^8 N/m
k_g	10^9 N/m	10^9 N/m	10^9 N/m	10^9 N/m
M_1	15.000 kg	15.000 kg	15.000 kg	15.000 kg
M_2	1.400 kg	1.400 kg	1.400 kg	1.400 kg
M_3	400 kg	400 kg	400 kg	360 kg
M_4	400 kg	400 kg	400 kg	340 kg
M_5, M_6	400 kg	400 kg	400 kg	400 kg

Table 3 shows the natural frequencies $\omega_i = \sqrt{\bar{k}_i / m_i}$ for each case, which corresponds to the peaks of the transfer functions in Figures 3–6. In equation (28), the DTF $T_{ij}^D = \bar{k}_{ij} / (\bar{k}_j - \omega^2 m_j)$, which shows T_{ij}^D reaches the peak at ω_i. In Figures 3–6 for transfer functions, each figure have 4 subplots for cases (a), (b), (c) and (d) respectively.

Table 3   Natural frequency values

Natural frequencies	Case (a)	Case (b)	Case (c)	Case (d)
ω_1	13 Hz	4 Hz	4 Hz	4 Hz
ω_2	50 Hz	86 Hz	88 Hz	86 Hz
ω_3.	253 Hz	264 Hz	266 Hz	278 Hz
ω_4	253 Hz	264 Hz	264 Hz	286 Hz
ω_5	253 Hz	264 Hz	264 Hz	264 Hz
ω_6	253 Hz	264 Hz	264 Hz	264 Hz

The global and direction transfer functions in Figures 3–6 show some peaks and valleys. The peaks in the GTF T_{ij}^G correspond to the resonances of the acceptance, which come from the denominators of its GTFs. The valleys comply with the anti-resonances of the cross-acceptance in the numerator of the GTFs, according to the explanation in reference (Vaitkus et al., 2019). It represents the natural frequency of the system. Since the definition of global and DTFs differ, the peak and valley values for the DTF T_{ij}^D are different from the global ones. The red solid curves present the GTF and the blue dashed ones denote the DTF in Figures 3–6.

For Figure 3, as the GTF from subsystem 3 to itself $T_{33}^G = 1$, that is wheel 1, then $20 * \log_{10}(T_{33}^G) = 0$ as shown with red solid curves. However, the DTF T_{33}^D is well defined

in a frequency range depending on the case, shown with blue dashed curves. Among the four cases, it reveals that case (a) has the lowest values of peaks and valleys. The frequency locations of the valleys and peaks differ from case (a) at 50Hz to the other cases around 85Hz. In case (d), 3 peaks and valleys appear due to the decrease of the mass values, at 264Hz, 278Hz and 286 Hz.

Figure 3 (a)–(d) The global and direct transfer function of subsystem 3 (wheel 1) for cases (a), (b), (c) and (d), respectively. The red lines represent T_{33}^{D}. The blue dashed lines represent T_{33}^{G} (see online version for colours)
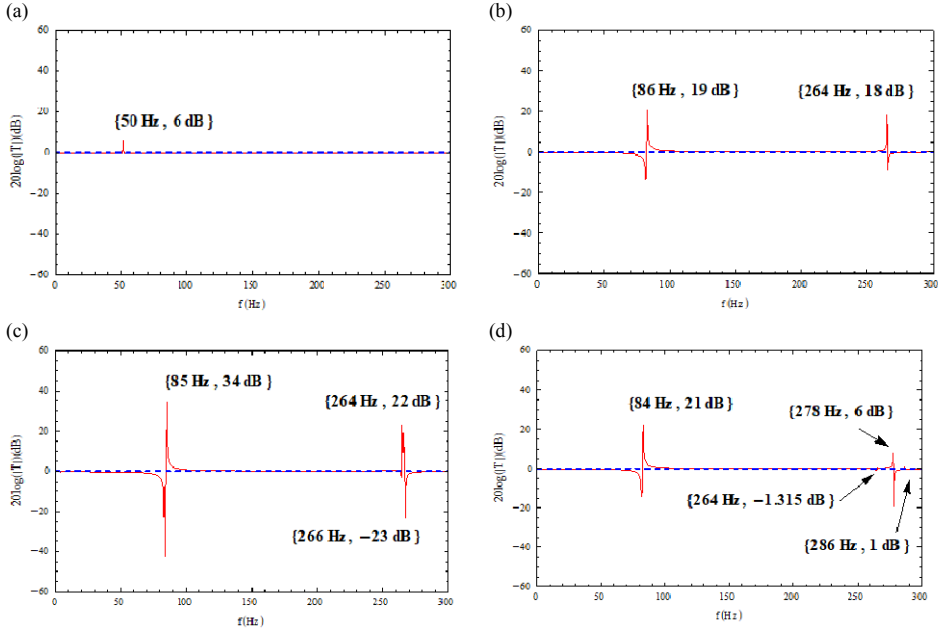
In Figure 4, the direct and GTFs T_{12}^{D} and T_{12}^{G} between subsystems 1 and 2, that is the vehicle body and bogie frame, are well defined and depend on the frequency in different shapes. Case (a) has the highest-level response for T_{12}^{D} in all frequency range, and the resonance frequency is at 50Hz. In case (d), two more peaks and valleys appear due to the decrease of the mass values, at 278 Hz and 286 Hz. As for the curves of T_{12}^{D} and T_{12}^{G}, they have different shapes, peaks, and valleys locations.

For Figure 5, $20\log_{10} T_{23}^{G,D}$ corresponds to DTFs between subsystems 2 and 3, which are the bogie mass M_{2} and wheel mass M_{3}. The shapes of both transfer functions are the same for all the frequency range. The peak levels and frequencies of the peak are slightly different from each other. Also, each peak represents one natural frequency of the system.

Figure 4   (a)- (d) the global and direct transfer function of subsystem 2 (bogie) to 1 (vehicle body) for cases (a), (b), (c) and (d), respectively. The red lines represent T_{12}^D. The blue dashed lines represent T_{12}^G (see online version for colours)
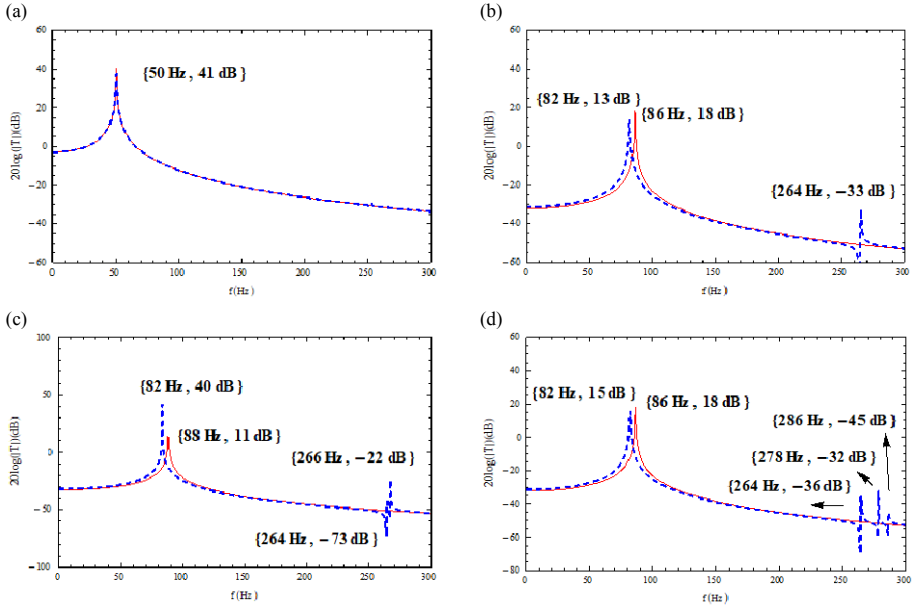
Figure 5   (a)–(d) The global and direct transfer function of subsystem 3 (wheel 1) to 2 (bogie) for cases (a), (b), (c) and (d), respectively. The red lines represent T_{23}^D. The blue dashed lines represent T_{23}^G (see online version for colours)
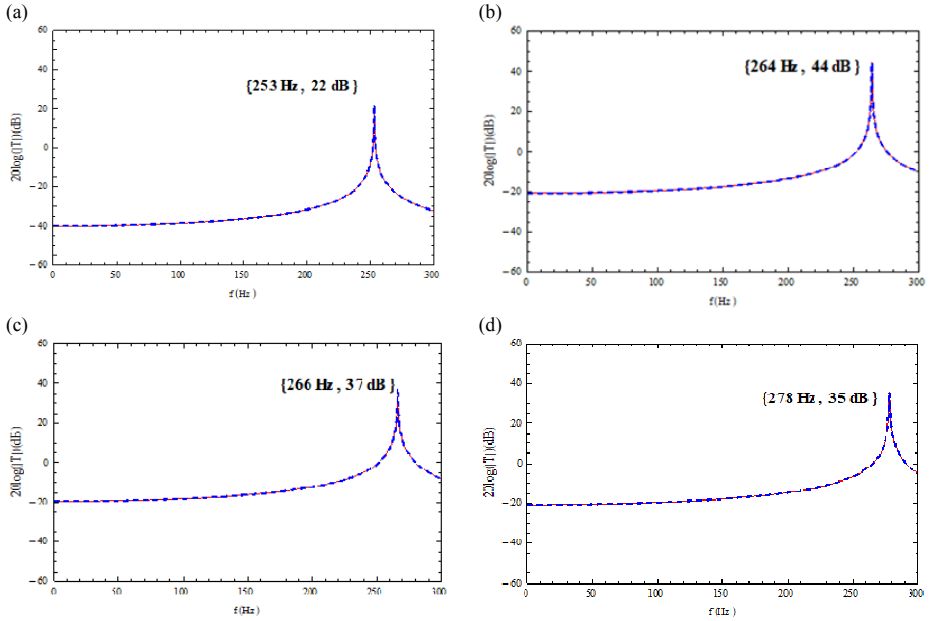
In Figure 6, as the masses of the vehicle body and the wheel M_3 are not directly connected, the DTF between subsystems 1 and 3 are $T_{13}^D = 0$, so its logarithm is $-\infty$. For GTF T_{13}^G, it's well defined. Compared to the figures above, the response levels are much lower. In case (c), GTF T_{13}^G shows a peak and valley at around 264 Hz and case (d) shows two more valleys and peaks compared to case (b) at around 278 Hz and 286 Hz.

Figure 6 (a)–(d) The global and direct transfer function of subsystem 3 (wheel 1) to 1 (vehicle body) cases (a), (b), (c) and (d), respectively. The blue dashed lines represent T_{13}^G (see online version for colours)
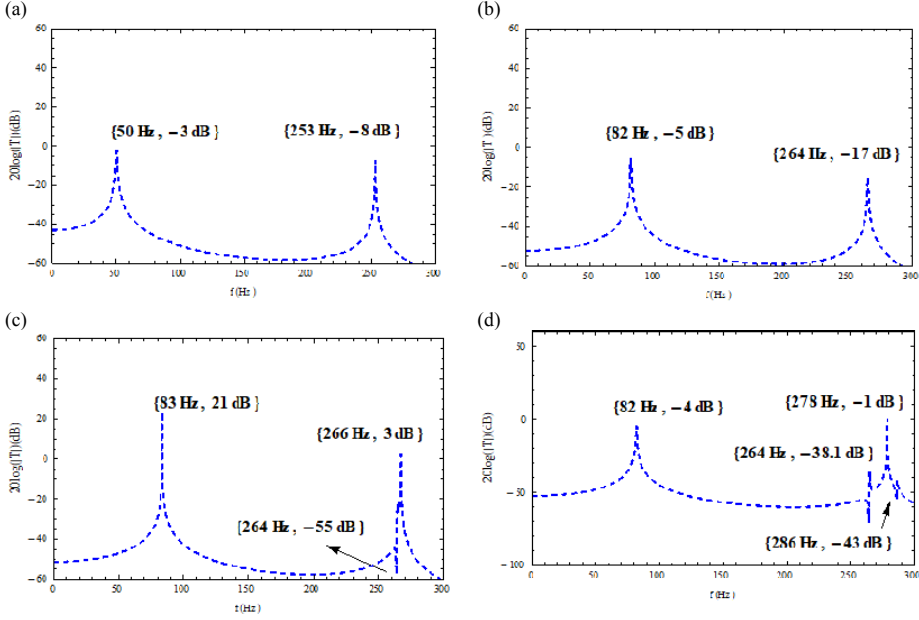
It can be observed that $T_{ij}^{G,D}$ transfer functions for any pair of subsystems, for the same case, have almost the same frequency peaks locations. After obtaining the global and DTF, it allows to investigate contribution of subsystems.

3.3 Contribution of subsystems

The whole system will vibrate when the railway vehicle is under operation. The motion of each subsystem can be obtained experimentally or analytically. In this study, the displacement of each subsystem is obtained from the motion equations (12)–(17). For the second part of the method, once the amplitude of the operational displacement of each subsystem is provided, the contributions due to each mass can be found out, according to equation (10):

$$Z_1^{op} = T_{21}^D * Z_2^{op} + T_{11}^D * Z_1^{op,ext} \tag{29}$$

$$Z_2^{op} = T_{12}^D * Z_1^{op} + T_{22}^D * Z_2^{op,ext} + T_{32}^D * Z_3^{op} + T_{42}^D * Z_4^{op} + T_{52}^D * Z_5^{op} + T_{62}^D * Z_6^{op} \tag{30}$$

$$Z_3^{op} = T_{23}^D * Z_2^{op} + T_{33}^D * Z_3^{op,ext} \tag{31}$$

$$Z_4^{op} = T_{24}^{D} * Z_2^{op} + T_{44}^{D} * Z_4^{op,ext} \tag{32}$$

$$Z_5^{op} = T_{25}^{D} * Z_2^{op} + T_{55}^{D} * Z_5^{op,ext} \tag{33}$$

$$Z_6^{op} = T_{26}^{D} * Z_2^{op} + T_{66}^{D} * Z_6^{op,ext} \tag{34}$$

Equations (29) to (34) are the displacement contribution for connected subsystems with an external force. For example, in equation (32), Z_4^{op} is factorised as a contribution due to the displacements of the bogie frame $T_{24}^{D} * Z_2^{op}$, plus the contribution of $T_{44}^{D} * Z_4^{op,ext}$ due to an external force applied over mass M_4. The value of the operational external signal $Z_i^{op,ext}, i = 1,2,3,4,5,6$ is according to the definition in equation (11).

As the motion equation in all the DOF were already established in the modelling, represented by Figure 1 and Table 1, it allows predicting the Transfer Paths among them according to the GTDT method. As shown in Figure 7, the external forces on the wheels, which are the subsystems 3, 4, 5, and 6, are considered. Subsystem 2 of the bogie is taken as the receiver, and the input vibration is contributed by subsystems 1, 3, 4, 5, 6 through paths 1, 2, 4, 6 and 8.

Figure 7   The signal transfer paths of all subsystems
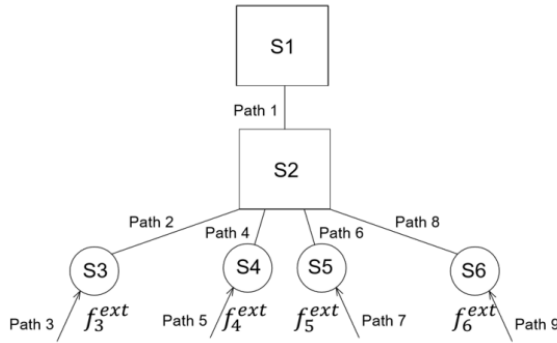
Assuming the four wheels have different irregularities during manufacture or operation defects, they are under excitations from the wheel-rail interaction. The external operational forces on the four wheels are f_3^{ext}, f_4^{ext}, f_5^{ext}, and f_6^{ext}, with amplitude values $F_{3,4,5,6}^{op} = (4 \times 10^4, \ 5 \times 10^4, 6 \times 10^4, 7 \times 10^4)^T$ respectively. Subsystem 6, which is the wheel 4, has the largest excitation amplitude. Owing to the excitations are from subsystems 3, 4, 5 and 6, the vibration transfers among the entire vehicle system.

According to the factorisation, equations (29), (30) and (32), Figures 8–10 display the operational response of the subsystem and the contribution of other systems to the system under consideration.

Figure 8 describes the contribution of the displacement amplitude of the vehicle body M_1 due to the bogie frame, which is the only mass directly connected to it. By equation (29), $Z_1^{op} = T_{21}^{D} \times Z_2^{op} + T_{11}^{D} \times Z_1^{op,ext}$. In the simulation, the excitation on subsystem 1 is not considered, which is $Z_1^{op,ext} = 0$. Then, $Z_1^{op} = T_{21}^{D} \times Z_2^{op}$. Therefore, red curves for Z_1^{op} and blue dashed for $T_{21}^{D} * Z_2^{op}$ coincide with each other.

Figure 8   (a)–(d) The contribution for subsystem 1 in cases (a), (b), (c) and (d), respectively. The red lines represent Z_1^{op}. The blue dashed lines represent $T_{21}^D \times Z_2^{op}$ (see online version for colours)
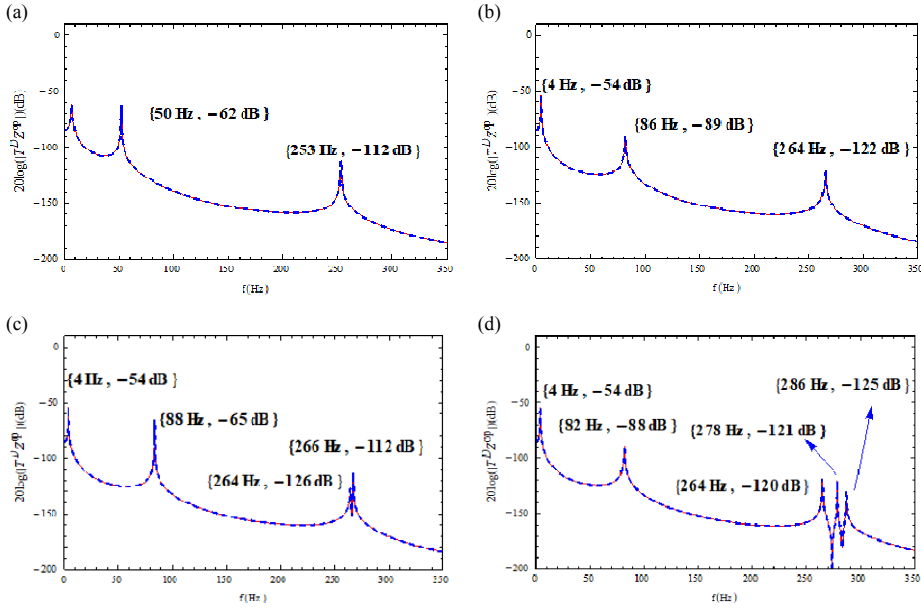
For case (d), as the masses M_3 and M_4 were decreased, it showed a different disturbance, between 264 Hz and 286 Hz, with 2 peaks and valleys that did not appear in case (c). Also, comparing case (c) with case (d), the second peak shows higher levels of displacement, due to the increase in k_{23} stiffness.

Figure 9 represents the contribution of the displacement amplitude Z_2^{op} of the bogie, due to the contribution of the wheels and the vehicle body. Also, besides each contribution curve, the values of each subsystem (dB) in resonance frequency are indicated.

For all cases, the wheel masses have the highest impact on the bogie displacement. The highest displacement contribution in most frequencies is due to wheel 4 M_6, which is subjected to the highest external force excitation. However, in case (a), the mass M_1 until 20 Hz has the highest degree of displacement level.

The maximum displacement of the bogie frame M_2 is in case (c), probably due to the increase of k_{23} stiffness. For case (d), the decrease of mass M_3 and M_4 led to a slight increase in the displacement contribution of these wheel masses around 270 Hz and a disturbance in the bogie displacement. Also, the change of the wheel masses leads to another peak around 286 Hz, in which masses M_3 and M_4 are responsible for the bogie frame displacement.

Figure 9   (a)–(d) The contribution for subsystem 2 in cases (a), (b), (c) and (d), respectively. The Z_2^{op} is marked as red lines. The $T_{12}^D \times Z_1^{op}$ is marked as black dashed lines. The $T_{32}^D \times Z_3^{op}$ is marked as yellow lines. The red dashed lines represent the $T_{42}^D \times Z_4^{op}$. The orange dashed lines represent the $T_{52}^D \times Z_5^{op}$. The $T_{62}^D \times Z_6^{op}$ is marked as black dotted lines (see online version for colours)

(a)
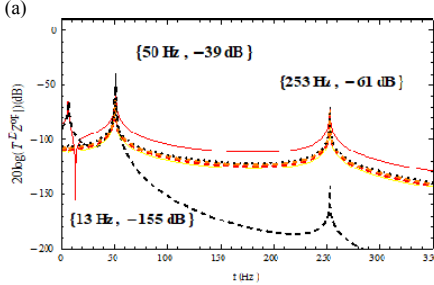
Subsystem.	50Hz	253Hz
Vehicle body	-39	-143
Wheel 1	-66	-74
Wheel 2	-64	-73
Wheel 3	-64	-71
Wheel 4	-62	-70

(b)
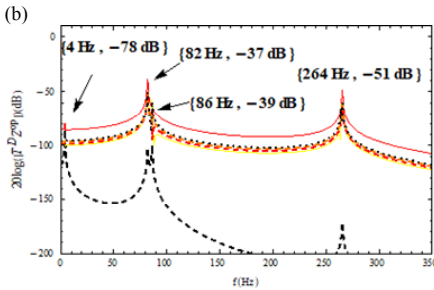
Subsystem.	82Hz	86Hz	264Hz
Vehicle body	-100	-102	-172
Wheel 1	-50	-57	-61
Wheel 2	-50	-65	-68
Wheel 3	-50	-71	-60
Wheel 4	-50	-59	-60

(c)
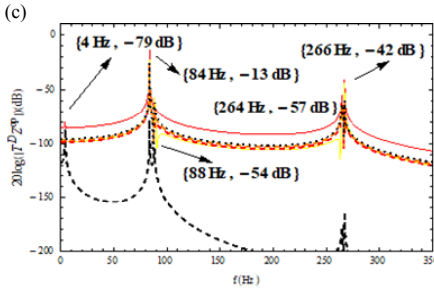
Subsystem	82Hz	86Hz	264Hz	266Hz
Vehicle body	-78	-104	-178	-163
Wheel 1	-23	-56	-65	-43
Wheel 2	-26	-74	-62	-60
Wheel 3	-26	-67	-62	-59
Wheel 4	-26	-62	-63	-60

(d)
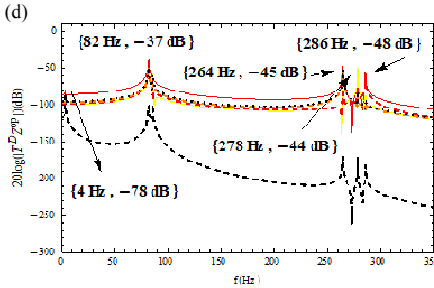
Subsystem	82 Hz	86 Hz	264 Hz	278 Hz	286 Hz
Vehicle body	-101	-100	-169	-172	-181
Wheel 1	-49	-57	-79	-47	-86
Wheel 2	-49	-65	-82	-75	-56
Wheel 3	-49	-71	-52	-82	-97
Wheel 4	-49	-59	-52	-82	-96

Figure 10 (a)–(d) The contribution for subsystem 4 in cases (a), (b), (c) and (d). The red lines represent Z_4^{op}. The blue dashed lines represent $T_{42}^D \times Z_2^{op}$ .1 $T_{44}^D \times Z_4^{op,ext}$ is marked as black dashed lines (see online version for colours)
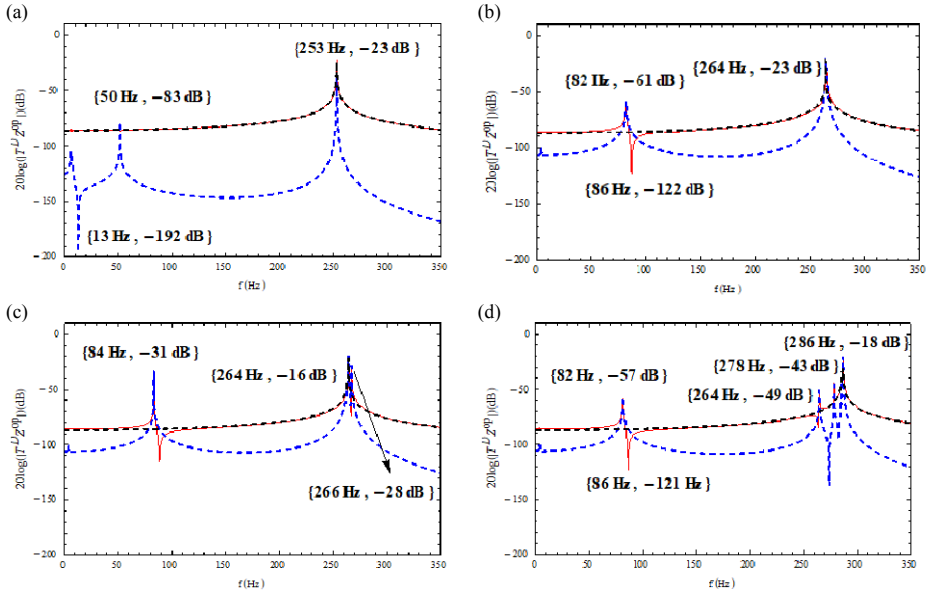
Figure 10 shows the displacement of the wheel M_4 which has the influence on the mass of the bogie frame and the external force over it. For cases (b), (c) and (d), around 82 Hz, there is a resonance of bogie frame and wheel. In all cases, the highest contribution comes from the external force over the wheel.

The bogie frame and the wheel are in resonance at different frequencies. In case (c) it is possible to see that at 84 Hz there is the highest displacement amplitude among the cases, due to the increase of stiffness k_{23}. Also for case (c), it shows a peak around 266 Hz, which did not appear in case (b). As for case (d) also 2 more locations of resonance appear, due to the lower wheel masses.

To validate equations (29)–(34), Figure 11(a)–(c) compare the sum of the displacement contributions in M_1, M_2 and M_4 subsystems with the actual operational displacement for case (d). All the curves overlap, which reveals the effectiveness of this TPA.

3.4 Results discussion

The curves for case (a) show different responses, because the secondary suspension spring stiffness represented by the parameter k_{12} is ten times higher than the primary suspension spring stiffness represented by the parameters k_{23}, k_{24}, k_{25} and k_{26}. In cases (b), (c) and (d), the stiffness k_{23} is higher than k_{12}. Case (d) shows the disturbances in all subsystem displacement amplitudes due to the decrease of the masses M_3 and M_4.

The result of factorisation above shows case (c) with overall higher displacements amplitudes, as the stiffness parameter k_{23} was 20% higher compared to cases (b) and (d).

Figure 11 (a)–(c) The displacement of mass M_1, M_2 and M_4, respectively. The synthetic displacements Z_i^{op} $(i = 1, 2, 4)$ are marked as red lines. The actual operational displacements $Z_i^{op'}$ $(i = 1, 2, 4)$ are marked as the blue dashed lines (see online version for colours)
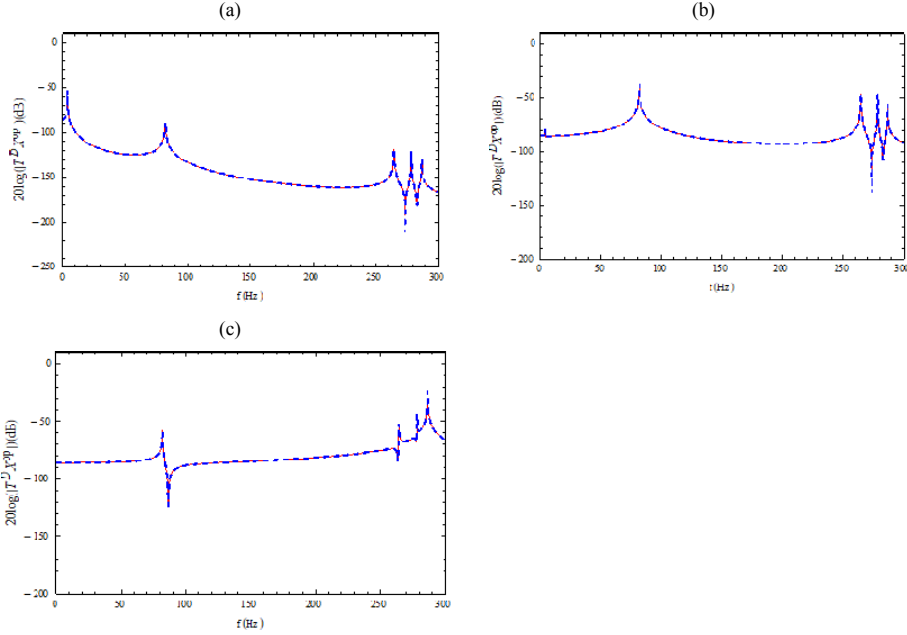
For all 4 cases, the external force acting over the wheel is responsible for the highest contribution levels of the bogie. Also, the mass decrease in case (d) incurs disturbances in the displacements in all subsystems. Concerning the vehicle body displacement, case (c) shows the highest displacement values. Also, the peak values in the $T_{ij}^{G,D}$ curves from Section 3.2 coincide with the resonance values in the curve of displacement in Section 3.3.

4   ATPA analysis of the railway vehicle with 11 DOF model

4.1   Mathematical model of a railway vehicle with 11 DOF

To make the model more complete, a mathematical model with 11 DOF for one entire railway vehicle is established, as shown in Figure 12. The symbols in the model are similar to those in Figure 1. M_1 denotes the vehicle body, and M_2 and M_3 denote the two bogies, M_4 to M_{11} are the eight wheels. $k_{24}, k_{25}, k_{26}, k_{27}, k_{38}, k_{39}, k_{310}, k_{311}$ are stiffness of the primary suspensions. k_{12} and k_{13} are the stiffness of the secondary

suspension. k_g is the contact stiffness between the wheel and rail. Only the vertical motions of the model are considered.

Figure 12 Physical model of a car with 11 DOF
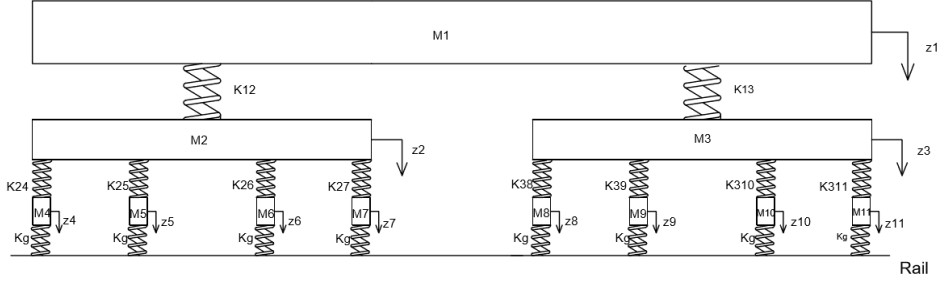
The governing equations of motion, according to the second Newton's law, are the following:

For the vehicle body M_1:

$$M_1 \ddot{z}_1 = F_{12} - F_{13} - f_1$$
$$M_1 \ddot{z}_1 = k_{12}(z_1 - z_2) - k_{13}(z_1 - z_3) - f_1$$

$$(35)$$

In equation (35), F_{12} and F_{13} are the restoring force of secondary suspension with stiffness k_{12} and k_{13}. M_1 is the vehicle body mass and f_1 is the external force as aerodynamic force or excitation from any device mounted to the vehicle body. Also, z_1 is the vehicle body vertical displacement, z_2 and z_3 are the bogie frame displacements.

For the 2 bogie frames:

$$M_2 \ddot{z}_2 = F_{23} + F_{24} + F_{25} + F_{26} - F_{12} - f_2$$
$$M_2 \ddot{z}_2 = k_{23}(z_2 - z_3) + k_{24}(z_2 - z_4) + k_{25}(z_2 - z_5) + k_{26}(z_2 - z_6) + k_{12}(z_1 - z_2) - f_2$$

$$(36)$$

In equation (36), F_{23}, F_{24}, F_{25} and F_{26} are the restoring forces of primary suspension with stiffness k_{23}, k_{24}, k_{25} and k_{26}. f_2 is the external force from the excitation of the motor or gearbox. Also, z_3, z_4, z_5 and z_6 are the displacements of the wheel.

$$M_3 \ddot{z}_3 = F_{38} + F_{39} + F_{310} + F_{311} - F_{13} - f_3$$
$$M_3 \ddot{z}_3 = k_{38}(z_3 - z_8) + k_{39}(z_3 - z_9) + k_{310}(z_3 - z_{10}) + k_{311}(z_3 - z_{11}) + k_{13}(z_3 - z_1) - f_3$$

$$(37)$$

In equation (37), F_{38}, F_{39}, F_{310} and F_{311} are the restoring forces with stiffness k_{38}, k_{39}, k_{310} and k_{311} acting over M_3. f_3 is the external force similar to f_2. Also, z_8, z_9, z_{10} and z_{11} are the displacements of each wheel. Each wheel is subjected to the contact force between wheel and rail interaction with stiffness k_g and the restoring force of primary suspension connected to the bogie frame.

$$M_4 \ddot{z}_4 = k_g z_4 - F_{24} - f_4$$
$$M_4 \ddot{z}_4 = k_g z_4 + k_{24}(z_4 - z_2) - f_4$$

$$(38)$$

$$M_5\ddot{z}_5 = k_g z_5 - F_{25} - f_5$$
$$M_5\ddot{z}_5 = k_g z_5 + k_5(z_5 - z_2) - f_5$$
(39)

$$M_6\ddot{z}_6 = k_g z_6 - F_{26} - f_6$$
$$M_6\ddot{z}_6 = k_g z_6 + k_{26}(z_6 - z_2) - f_6$$
(40)

$$M_7\ddot{z}_7 = k_g z_7 - F_{27} - f_7$$
$$M_7\ddot{z}_7 = k_g z_7 + k_{27}(z_7 - z_2) - f_7$$
(41)

For equations (38)–(41), M_4, M_5, M_6 and M_7 are the masses of the wheels of the bogie M_2.

$$M_8\ddot{z}_8 = k_g z_8 - F_{28} - f_8$$
$$M_8\ddot{z}_8 = k_g z_8 + k_{28}(z_8 - z_2) - f_8$$
(42)

$$M_9\ddot{z}_9 = k_g z_9 - F_{29} - f_9$$
$$M_9\ddot{z}_9 = k_g z_9 + k_{29}(z_9 - z_2) - f_9$$
(43)

$$M_{10}\ddot{z}_{10} = k_g z_{10} - F_{210} - f_{10}$$
$$M_{10}\ddot{z}_{10} = k_g z_{10} + k_{210}(z_{10} - z_2) - f_{10}$$
(44)

$$M_{11}\ddot{z}_{11} = k_g z_{11} - F_{211} - f_{11}$$
$$M_{11}\ddot{z}_{11} = k_g z_{11} + k_{211}(z_{11} - z_2) - f_{11}$$
(45)

For equations (42)–(45), M_8, M_9, M_{10} and M_{11} are the masses of the wheels of the bogie M_3. For each wheel, it is subjected to the contact force from wheel and rail interaction with stiffness k_g and the restoring force of primary suspension connected to the bogie frame.

The model has 11 subsystems, as represented in Table 4.

Table 4   Description of subsystems

Subsystem number	1	2	3	4	5	6
Subsystems	Half vehicle body	Bogie frame 1	Bogie frame 2	Wheel 1	Wheel 2	Wheel 3
Subsystem number	7	8	9	10	11	
Subsystems	Wheel 4	Wheel 5	Wheel 6	Wheel 7	Wheel 8	

4.2   GTF and DTF of 11 DOF model

Figure 13(a) illustrates the global transfer relations for the entire car model with 11 DOF, and the GTFs analysed in the following figures are highlighted in red dashed. Like Section 3, the DTFs are represented in Figure 13(b), considering the external force over all the wheels. It shows the direct connections between subsystems which are calculated after the GTFs are obtained.

Figure 13 (a) Global Transfer Functions among all subsystems. (b) Direct Transfer Functions between 2 direct connected subsystems (see online version for colours)

(a)   (b)
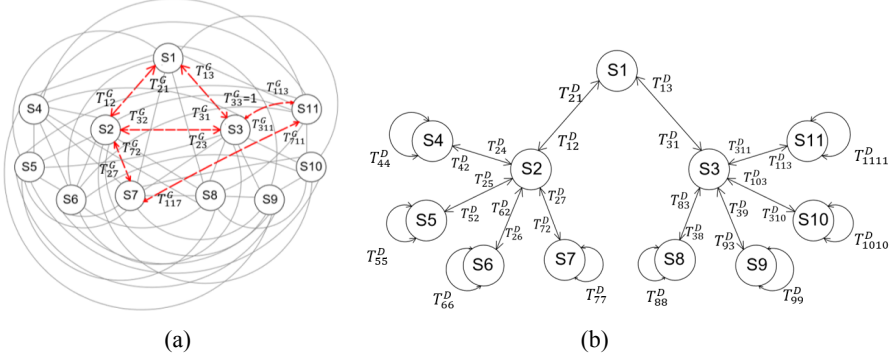
The same procedure from Section 3.1 for 11 DOF was done. The mass and stiffness matrix are the following:

$$\overline{\mathbf{M}} = \begin{pmatrix}
M_1 & 0 & 0 & 0 & 0 & 0 & 0 & 0 & 0 & 0 \\
0 & M_2 & 0 & 0 & 0 & 0 & 0 & 0 & 0 & 0 \\
0 & 0 & M_3 & 0 & 0 & 0 & 0 & 0 & 0 & 0 \\
0 & 0 & 0 & M_4 & 0 & 0 & 0 & 0 & 0 & 0 \\
0 & 0 & 0 & 0 & M_5 & 0 & 0 & 0 & 0 & 0 \\
0 & 0 & 0 & 0 & 0 & M_6 & 0 & 0 & 0 & 0 \\
0 & 0 & 0 & 0 & 0 & 0 & M_7 & 0 & 0 & 0 \\
0 & 0 & 0 & 0 & 0 & 0 & 0 & M_8 & 0 & 0 \\
0 & 0 & 0 & 0 & 0 & 0 & 0 & 0 & M_9 & 0 \\
0 & 0 & 0 & 0 & 0 & 0 & 0 & 0 & 0 & M_{11}
\end{pmatrix} \tag{46}$$

For the stiffness matrix:

$$\overline{\mathbf{K}} = \begin{pmatrix}
\overline{k}_1 & \overline{k}_{12} & \overline{k}_{13} & 0 & 0 & 0 & 0 & 0 & 0 & 0 & 0 \\
\overline{k}_{12} & \overline{k}_2 & \overline{k}_{23} & \overline{k}_{24} & \overline{k}_{25} & \overline{k}_{26} & \overline{k}_{27} & 0 & 0 & 0 & 0 \\
\overline{k}_{13} & \overline{k}_{23} & \overline{k}_3 & 0 & 0 & 0 & 0 & \overline{k}_{38} & \overline{k}_{39} & \overline{k}_{310} & \overline{k}_{311} \\
0 & \overline{k}_{24} & 0 & \overline{k}_4 & 0 & 0 & 0 & 0 & 0 & 0 & 0 \\
0 & \overline{k}_{25} & 0 & 0 & \overline{k}_5 & 0 & 0 & 0 & 0 & 0 & 0 \\
0 & \overline{k}_{26} & 0 & 0 & 0 & \overline{k}_6 & 0 & 0 & 0 & 0 & 0 \\
0 & \overline{k}_{27} & 0 & 0 & 0 & 0 & \overline{k}_7 & 0 & 0 & 0 & 0 \\
0 & 0 & \overline{k}_{38} & 0 & 0 & 0 & 0 & \overline{k}_8 & 0 & 0 & 0 \\
0 & 0 & \overline{k}_{39} & 0 & 0 & 0 & 0 & 0 & \overline{k}_9 & 0 & 0 \\
0 & 0 & \overline{k}_{310} & 0 & 0 & 0 & 0 & 0 & 0 & \overline{k}_{10} & 0 \\
0 & 0 & \overline{k}_{311} & 0 & 0 & 0 & 0 & 0 & 0 & 0 & \overline{k}_{11}
\end{pmatrix} \tag{47}$$

For the problem stated:

$$\bar{k}_1 = \bar{k}_{12} + \bar{k}_{13}; \bar{k}_2 = \bar{k}_{23} + \bar{k}_{24} + \bar{k}_{25} + \bar{k}_{26} + \bar{k}_{12}; \bar{k}_3 = \bar{k}_{38} + \bar{k}_{39} + \bar{k}_{310} + \bar{k}_{311} + \bar{k}_{13};$$

$$\bar{k}_4 = \bar{k}_{24} + \bar{k}_g; \bar{k}_5 = \bar{k}_{25} + \bar{k}_g;$$

$$\bar{k}_6 = \bar{k}_{26} + \bar{k}_g; \bar{k}_7 = \bar{k}_{27} + \bar{k}_g; \bar{k}_8 = \bar{k}_{28} + \bar{k}_g; \bar{k}_9 = \bar{k}_{29} + \bar{k}_g; \bar{k}_{10} = \bar{k}_{210} + \bar{k}_g;$$

$$\bar{k}_{11} = \bar{k}_{211} + \bar{k}_g;$$

For the dynamic stiffness matrix:

$$\bar{\mathbf{K}} = \begin{pmatrix} K_1 & -\bar{k}_{12} & -\bar{k}_{13} & 0 & 0 & 0 & 0 & 0 & 0 & 0 & 0 \\ -\bar{k}_{12} & K_2 & -\bar{k}_{23} & -\bar{k}_{24} & -\bar{k}_{25} & -\bar{k}_{26} & -\bar{k}_{27} & 0 & 0 & 0 & 0 \\ -\bar{k}_{13} & -\bar{k}_{23} & K_3 & 0 & 0 & 0 & 0 & -\bar{k}_{38} & -\bar{k}_{39} & -\bar{k}_{310} & -\bar{k}_{311} \\ 0 & -\bar{k}_{24} & 0 & K_4 & 0 & 0 & 0 & 0 & 0 & 0 & 0 \\ 0 & -\bar{k}_{25} & 0 & 0 & K_5 & 0 & 0 & 0 & 0 & 0 & 0 \\ 0 & -\bar{k}_{26} & 0 & 0 & 0 & K_6 & 0 & 0 & 0 & 0 & 0 \\ 0 & -\bar{k}_{27} & 0 & 0 & 0 & 0 & K_7 & 0 & 0 & 0 & 0 \\ 0 & 0 & -\bar{k}_{38} & 0 & 0 & 0 & 0 & K_8 & 0 & 0 & 0 \\ 0 & 0 & -\bar{k}_{39} & 0 & 0 & 0 & 0 & 0 & K_9 & 0 & 0 \\ 0 & 0 & -\bar{k}_{310} & 0 & 0 & 0 & 0 & 0 & 0 & K_{10} & 0 \\ 0 & 0 & -\bar{k}_{311} & 0 & 0 & 0 & 0 & 0 & 0 & 0 & K_{11} \end{pmatrix}$$

$$(48)$$

where $K_i = \bar{k}_i - M_i \omega^2, (i = 1, 2, ..., 11)$. The GTF matrix has a dimension of 11×11 and is obtained as a matrix (25), in the previous section. To obtain the DTF matrix, the non-diagonal elements must be considered:

$$T_{14}^D = T_{15}^D = T_{16}^D = T_{17}^D = T_{18}^D = T_{19}^D = T_{110}^D = T_{111}^D = T_{23}^D = T_{28}^D = T_{29}^D = T_{210}^D$$

$$= T_{211}^D = T_{32}^D = T_{34}^D = T_{35}^D = T_{36}^D = T_{37}^D = T_{41}^D = T_{42}^D = T_{43}^D = T_{45}^D = T_{46}^D = T_{47}^D$$

$$= T_{48}^D = T_{49}^D = T_{410}^D = T_{411}^D = T_{51}^D = T_{53}^D = T_{54}^D = T_{56}^D = T_{57}^D = T_{58}^D = T_{59}^D = T_{510}^D$$

$$= T_{511}^D = T_{61}^D = T_{63}^D = T_{65}^D = T_{67}^D = T_{68}^D = T_{69}^D = T_{610}^D = T_{611}^D = T_{71}^D = T_{73}^D = T_{74}^D$$

$$= T_{75}^D = T_{76}^D = T_{78}^D = T_{79}^D = T_{710}^D = T_{711}^D = T_{81}^D = T_{82}^D = T_{84}^D = T_{85}^D = T_{86}^D = T_{87}^D$$

$$= T_{89}^D = T_{810}^D = T_{811}^D = T_{91}^D = T_{92}^D = T_{94}^D = T_{95}^D = T_{96}^D = T_{97}^D = T_{98}^D = T_{910}^D = T_{911}^D$$

$$= T_{101}^D = T_{102}^D = T_{104}^D = T_{105}^D = T_{106}^D = T_{107}^D = T_{108}^D = T_{109}^D = T_{1011}^D = T_{111}^D = T_{112}^D = T_{114}^D$$

$$= T_{115}^D = T_{116}^D = T_{117}^D = T_{118}^D = T_{119}^D = T_{1110}^D = 0$$

For the diagonal elements, the expression T_{ii}^D was already explained in equation (27) and for the non-diagonal elements equation (28). The values of masses and the spring stiffness are shown in Table 5, and 2 cases will be analysed. The model with parameters in case (a) is a symmetric one, where each bogie, wheel and corresponding suspension are in an ideal state with the same parameters. In case (b), some parameters have a little deviation from the ideal state to show the effect of structure parameters change on the

transfer function. Stiffness k_{13} in case (b) is 20% lower than that in case (a), k_{27} is 20% higher and k_{311} is 10% lower than case (a). For the masses, for case (b) M_7 is 10% lower and M_{11} 15% than case (a).

Table 5   Variable values

Variables	Case (a)	Case (b)
k_{12}	$10^7\,\text{N/m}$	$10^7\,\text{N/m}$
k_{13}	$10^7\,\text{N/m}$	$0.8\times10^7\,\text{N/m}$
$k_{24}\,/\,k_{25}\,/\,k_{26}$	$10^8\,\text{N/m}$	$10^8\,\text{N/m}$
k_{27}	$10^8\,\text{N/m}$	$1.2\times10^8\,\text{N/m}$
$k_{38}\,/\,k_{39}\,/\,k_{310}$	$10^8\,\text{N/m}$	$0.9\times10^8\,\text{N/m}$
k_{311}	$10^8\,\text{N/m}$	$0.9\times10^8\,\text{N/m}$
k_g	$10^9\,\text{N/m}$	$10^9\,\text{N/m}$
M_1	30kg	30kg
M_2	1.4kg	1.4kg
M_3	1.4kg	1.26kg
$M_4\,/\,M_5\,/\,M_6$	400kg	400kg
M_7	400kg	360kg
$M_8\,/\,M_9\,/\,M_{10}$	400kg	400kg
M_{11}	400kg	340kg

Table 6 shows the natural frequencies $\omega_i = \sqrt{k_i / m_i}$ for each case, in Hertz, which correspond to the peaks and valleys of Figures 15 and 16.

4.3   Contribution of subsystems

When the vehicle is under excitation, the whole system will vibrate. The motion of each subsystem can be obtained experimentally or analytically. In this study, the displacement of each subsystem is obtained from the motion equation (35) to (45). Once the operational displacements of each subsystem are provided, the contributions due to each mass are the following:

$$Z_1^{op} = T_{11}^{D} * Z_1^{op,ext} + T_{21}^{D} * Z_2^{op} + T_{31}^{D} * Z_3^{op} \tag{49}$$

$$Z_2^{op} = T_{12}^{D} * Z_1^{op} + T_{22}^{D} * Z_2^{op,ext} + T_{42}^{D} * Z_4^{op} + T_{52}^{D} * Z_5^{op} + T_{62}^{D} * Z_6^{op} + T_{72}^{D} * Z_7^{op} \tag{50}$$

$$Z_3^{op} = T_{13}^{D} * Z_1^{op} + T_{33}^{D} * Z_3^{op,ext} + T_{83}^{D} * Z_8^{op} + T_{93}^{D} * Z_9^{op} + T_{103}^{D} * Z_{10}^{op} + T_{113}^{D} * Z_{11}^{op} \tag{51}$$

$$Z_4^{op} = T_{24}^D * Z_2^{op} + T_{44}^D * Z_4^{op,ext} \tag{52}$$

$$Z_5^{op} = T_{25}^D * Z_2^{op} + T_{55}^D * Z_5^{op,ext} \tag{53}$$

$$Z_6^{op} = T_{26}^D * Z_2^{op} + T_{66}^D * Z_6^{op,ext} \tag{54}$$

$$Z_7^{op} = T_{27}^D * Z_2^{op} + T_{77}^D * Z_7^{op,ext} \tag{55}$$

$$Z_8^{op} = T_{38}^D * Z_3^{op} + T_{88}^D * Z_8^{op,ext} \tag{56}$$

$$Z_9^{op} = T_{39}^D * Z_3^{op} + T_{99}^D * Z_9^{op,ext} \tag{57}$$

$$Z_{10}^{op} = T_{310}^D * Z_3^{op} + T_{1010}^D * Z_{10}^{op,ext} \tag{58}$$

$$Z_{11}^{op} = T_{311}^D * Z_3^{op} + T_{1111}^D * Z_{11}^{op,ext} \tag{59}$$

In the simulations, the external operational force acting on the wheel masses are considered as $F_{1,2,3,4,5,6,7,8,9,10,11}^{op} = \left(0,0,0,4\times10^4,5\times10^4,6\times10^4,7\times10^4,8\times10^4,9\times10^4,10\times10^4,11\times10^4\right)^T$. It shows the eight wheels are under excitation with different amplitude and system 11 is under the largest excitation.

Table 6   Natural frequencies values

Natural frequencies	Case (a)	Case (b)
ω_1	4 Hz	4 Hz
ω_2	86 Hz	88 Hz
ω_3	86 Hz	89 Hz
ω_4	264 Hz	264 Hz
ω_5	264 Hz	264 Hz
ω_6	264 Hz	264 Hz
ω_7	264 Hz	281 Hz
ω_8	264 Hz	264 Hz
ω_9	264 Hz	264 Hz
ω_{10}	264 Hz	264 Hz
ω_{11}	264 Hz	285 Hz

Figure 14 shows the transfer path for the 11 DOF mechanical railway vehicle system, considering the external force over the wheel's masses. To analyse subsystem 1 as the receiver, the input is provided by subsystems 2 and 3, through Path 1 and 2. The external forces are f_4^{ext}, f_5^{ext}, f_6^{ext}, f_7^{ext}, f_8^{ext}, f_9^{ext}, f_{10}^{ext}, f_{11}^{ext}.

Figure 14 ATPA path analysis (see online version for colours)
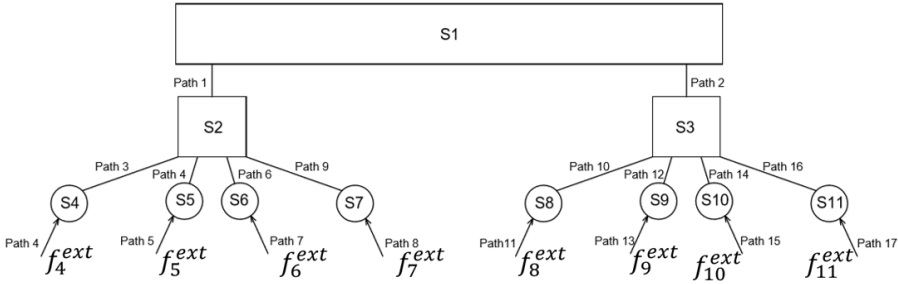
Figure 15(a) and (b) describe the contribution of the displacement of the vehicle body Z_1^{op} due to M_3 and M_2 bogie masses directly connected. The peak values represent the resonance of the subsystems. For case (a) the contribution from M_3 is slightly higher than that from mass M_2 in all frequency ranges, as the excitation forces transferring through the wheel M_3 are higher than over M_2. Case (b) shows two more resonance peaks at 281 Hz and 285 Hz that do not appear in case (a), due to the different parameter's values.

Figure 15(c) and (d) represent the contribution of the displacement Z_2^{op} of the bogie, due to the wheels and the vehicle body. The biggest contribution in most of the frequencies is due to the masses of the wheel M_7, which has the highest external force applied. Case (b) shows one more resonance frequency at 281 Hz compared with case (a).

Figure 15(e) and (f) represent the contribution of the displacement Z_3^{op} of the bogie, due to the wheels and the vehicle body. The highest contribution in all frequencies is due to the mass M_{11}, which is where the highest external force is applied. The results are similar to Figure 15(c) and (d).

Figure 16(a) and (b) are the operational displacements of the subsystem M_7. The displacement contribution for the wheel is due to the bogie M_2, as it is the only mass directly connected to it and due to the external force acting over it. For case (b), one more resonance is added, at 281 Hz, due to a change of the parameter's values.

Figure 16(c) and (d) show the operational displacement of the subsystem M_{11}. The displacement contribution for the wheel is due to the mass of the bogie M_3 and the external force acting over it. The results are similar to Figure 16(a) and (b). It is possible to realise that case (b) has higher values of displacements, due to the change of the parameters. Also, the overall displacement amplitudes are higher than the values of wheel M_7.

4.4   Results discussion

The result of factorisation above shows cases (a) and (b) using different stiffness, bogie and wheel masses. Also, the stiffness of primary and secondary spring suspensions is equal or very close to Case (b) in Section 3.3. Because of this, the shape and values of displacement contributions are very similar.

Figure 15 (a), (b) The contribution for subsystem 1 in case (a) and (b), respectively. The Z_1^{op} is marked as red lines. The black lines represent the $T_{21}^D \times Z_2^{op}$. The blue dashed lines mean the $T_{31}^D \times Z_3^{op}$. (c), (d) The contributions for subsystem 2 of the case (a) and (b), respectively. The red lines mean the Z_2^{op}. The $T_{12}^D \times Z_1^{op}$ is marked as orange dashed lines. The yellow lines represent the $T_{42}^D \times Z_4^{op}$. The green dashed lines mean the $T_{52}^D \times Z_5^{op}$. The $T_{62}^D \times Z_6^{op}$ is marked as blue dashed lines. The $T_{72}^D \times Z_7^{op}$ is marked as black dashed lines. (e) and (f) are the contributions for subsystem 3 of the case (a) and (b), respectively. The Z_3^{op} is marked as red lines. The orange dashed lines represent the $T_{13}^D \times Z_1^{op}$. The yellow lines mean $T_{38}^D \times Z_8^{op}$. The $T_{93}^D \times Z_9^{op}$ is marked as green lines. The $T_{310}^D \times Z_{10}^{op}$ is marked as blue dot-dashed. The black dashed lines represent the $T_{311}^D \times Z_{11}^{op}$ (see online version for colours)
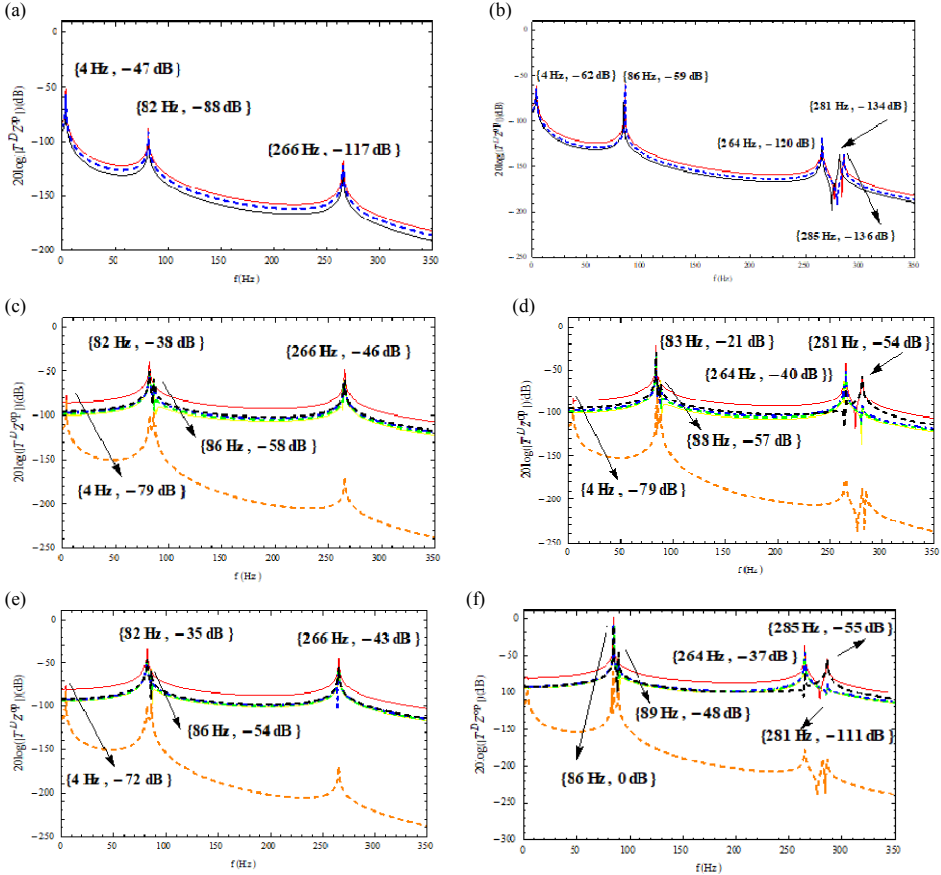
For the 2 cases, the external force acting over the wheel was responsible for the highest contribution levels in the bogie. Also, the decrease of the masses M_7 and M_{11} in case (b), like Section 3.1, caused disturbances in the displacement responses in the vehicle body and bogie frame M_2 and M_3. The change in the stiffness also influences the increase of the values of the displacement in the resonance, when comparing cases (a) and (b), especially in the second resonance peak.

Figure 16 (a) and (b) The contributions for subsystem 7 of the case (a) and (b), respectively. The Z_7^{op} is marked as red lines. The black dashed lines represent the $T_{72}^D \times Z_2^{op}$. The $T_{77}^D \times Z_7^{op,ext}$ is marked as blue dashed lines. (c), (d) The contributions for subsystem 11 of the case (a) and (b), respectively. The Z_{11}^{op} is marked as red lines. The black dashed represent the $T_{113}^D \times Z_3^{op}$. The blue dashed represent the $T_{1111}^D \times Z_{11}^{op,ext}$ (see online version for colours)
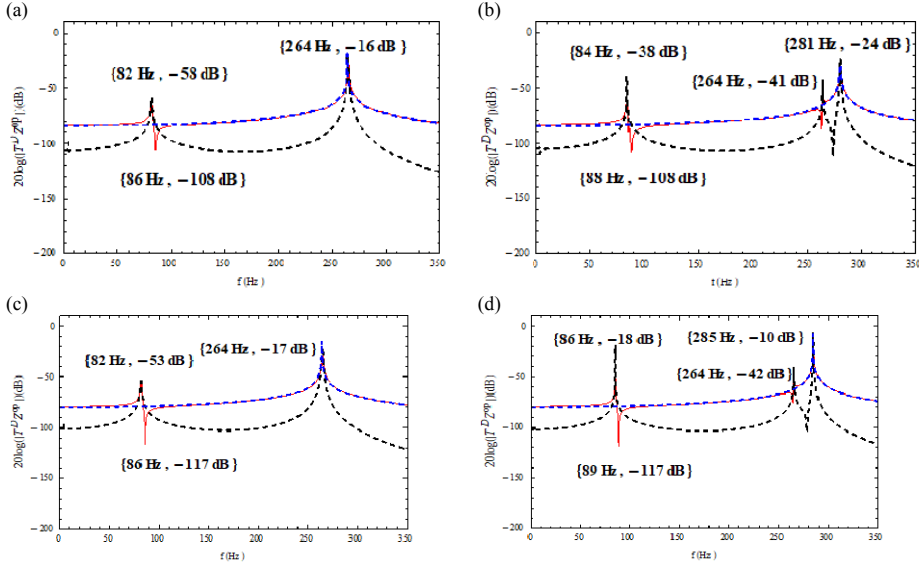
For both 6 DOF and 11 DOF models, different parameters of mass and stiffness in the primary suspension can increase the value of responses and cause disturbances in all the subsystems. Most importantly, for both physical models, the change in the wheel masses are the cause of the appearance of a new resonance frequency which can lead to damage in the system.

5 Conclusion

This paper aims to validate and demonstrate the effectiveness of the DTFs to determine the influence of displacements among the most important subsystems. It proves that the displacement of any subsystem can be factorised in terms of displacements of subsystems directly connected plus the displacement due to an external force.

The railway vehicle is modelled as a 6 DOF and 11 DOF mechanical system and the ATPA method is used to analyse the vertical displacements at different frequencies. For the 6 DOF model, four cases with different structure parameters are compared and the effects of the parameters on the transfer functions are discussed. Two cases with different system parameters are analysed for the 11 DOF model to show the effect of stiffness and masses change on the response of the vehicle body. Also, the half and entire models of the railway vehicle are compared to figure out whether the half model is feasible for the analysis, as it will save computational resources. For both models, different parameters of mass and stiffness in the primary suspension can increase the value of responses and

cause disturbances in all the subsystems. Also, when the stiffness of the secondary suspension is higher than the primary suspension the result in the bogie response will be different if it is the contrary. Most importantly, for both physical models, the change in the wheel masses are the cause of the appearance of a new resonance frequency which can lead to damage in the system.

It is possible to find from which subsystem the biggest contribution comes by using the GTDT method in a mechanical system. Therefore, the problematic equipment or component can be removed or improved to reduce its influence on the total displacement. Applying the method in a railway vehicle, the source of the disturbance to the vehicle body can be detected, if it is due to aerodynamic force, equipment's below or over the floor/roof or the contact between the wheel and the rail.

Acknowledgements

References

Aragonès, À., Poblet-Puig, J., Arcas, K., Rodríguez, P.V., Magrans, F.X. and Rodríguez-Ferran, A. (2019) 'Experimental and numerical study of advanced transfer path analysis applied to a box prototype', *Mechanical Systems and Signal Processing*, Vol. 114, pp.448–466.

Cao, Y., Li, Z., Ji, W. and Ma, M. (2021) 'Characteristics analysis of near-field and far-field aerodynamic noise around high-speed railway bridge', *Environ Sci Pollut Res Int*, Vol. 28, pp.29467–29483.

De Klerk, D. and Ossipov, A. (2010) 'Operational transfer path analysis: theory, guidelines and tire noise application', *Mechanical Systems and Signal Processing*, Vol. 24, pp.1950–1962.

Guasch, O. (2009) 'Direct transfer functions and path blocking in a discrete mechanical system', *Journal of Sound and Vibration*, Vol. 321, pp.854–874.

Jin, J., Yang, W., Koh, H-I. and Park, J. (2020) 'Development of tuned particle impact damper for reduction of transient railway vibrations', *Applied Acoustics*, Vol. 169, p.107487.

Lee, D. and Lee, J.W. (2020) 'Operational transfer path analysis based on deep neural network: numerical validation', *Journal of Mechanical Science and Technology*, Vol. 34, pp.1023–1033.

Ling, L., Jiang, P., Wang, K. and Zhai, W. (2020) 'Dynamic interaction between rail vehicles and vibration-attenuating slab tracks', *Construction and Building Materials*, Vol. 258, p.119545.

Liu, N., Sun, Y., Wang, Y., Sun, P., Li, W. and Guo, H. (2020a) 'Mechanism of interior noise generation in high-speed vehicle based on anti-noise operational transfer path analysis', *Proceedings of the Institution of Mechanical Engineers, Part D: Journal of Automobile Engineering*, Vol. 235, pp.273–287.

Liu, Q., Thompson, D.J., Xu, P., Feng, Q. and Li, X. (2020b) 'Investigation of train-induced vibration and noise from a steel-concrete composite railway bridge using a hybrid finite element-statistical energy analysis method', *Journal of Sound and Vibration*, Vol. 471, p.115197.

Liu, S. (2020) 'RETRACTED: measurement and analysis of vibration and noise in the ambient environment of metro', *Measurement*, p.163.

Lv, R., Yuan, Z., Lei, B., Zheng, J. and Luo, X. (2021) 'Model predictive control with adaptive building model for heating using the hybrid air-conditioning system in a railway station', *Energies*, Vol. 14, No. 7, p.1996.

Magrans, F.X. (1981) 'Method of measuring transmission paths', *Journal of Sound and Vibration*, Vol. 74, pp.321–330.

Magrans, F.X. (1984) 'Direct transference applied to the study of room acoustics', *Journal of Sound and Vibration*, Vol. 96, pp.13–21.

Meggitt, J.W.R., Elliott, A.S., Moorhouse, A.T., Jalibert, A. and Franks, G. (2021) 'Component replacement TPA: a transmissibility-based structural modification method for in-situ transfer path analysis', *Journal of Sound and Vibration*, Vol. 499, p.115991.

Moghaddam, A.K. (2017) 'A review on the current methods of railway induced vibration attenuations', *International Journal of Science and Engineering Applications*, Vol. 6, pp.123–128.

Oktav, A., Yilmaz, Ç. and Anlaş, G. (2017) 'Transfer path analysis: current practice, trade-offs and consideration of damping', *Mechanical Systems and Signal Processing*, Vol. 85, pp.760–772.

Song, L., Gui, Q., Chen, H., Bai, H. and Sun, Y. (2021) 'Operational transfer path analysis based on signal decoupling', *Journal of Vibration and Acoustics,* 143.

Vaitkus, D., Tcherniak, D. and Brunskog, J. (2019) 'Application of vibro-acoustic operational transfer path analysis', *Applied Acoustics*, Vol. 154, pp.201–212.

Van Der Seijs, M.V., De Klerk, D. and Rixen, D.J. (2016) 'General framework for transfer path analysis: history, theory and classification of techniques', *Mechanical Systems and Signal Processing*, Vols. 68–69, pp.217–244.

Wei, K., Zhao, Z., Du, X., Li, H. and Wang, P. (2019) 'A theoretical study on the train-induced vibrations of a semi-active magneto-rheological steel-spring floating slab track', *Construction and Building Materials*, Vol. 204, pp.703–715.

Xia, E., Cao, Z., Zhu, X., Qiu, S., Xue, Z., He, H. and Li, L. (2021) 'A modified dynamic stiffness calculation method of rubber isolator considering frequency, amplitude and preload dependency and its application in transfer path analysis of vehicle bodies', *Applied Acoustics*, Vol. 175, p.107780.

Zhang, Z., Pan, D., Wu, W. and Huang, C. (2019) 'Vibration source identification of a heavy commercial vehicle cab based on operational transfer path analysis', *Proceedings of the Institution of Mechanical Engineers, Part D: Journal of Automobile Engineering*, Vol. 234, pp.669–680.